

Polarization control and tuning efficiency of tunable vertical-cavity surface-emitting laser with internal-cavity sub-wavelength grating*

Xiao-Long Wang(王小龙), Yong-Gang Zou(邹永刚)[†], Zhi-Fang He(何志芳),
Guo-Jun Liu(刘国军)[‡], and Xiao-Hui Ma(马晓辉)[§]

State Key Laboratory of High-Power Laser Diodes, Changchun University of Science and Technology, Changchun 130022, China

(Received 14 January 2020; revised manuscript received 23 April 2020; accepted manuscript online 19 May 2020)

We design an 850 nm tunable vertical-cavity surface-emitting laser (VCSEL) structure using an internal-cavity sub-wavelength grating. The use of such a tuning structure allows for wider wavelength tuning range and more stable single-polarization as compared to conventional tunable VCSELs. The features of the internal-cavity grating effect on the wavelength tuning and polarization characteristics of the tunable VCSEL are analyzed. The simulation results show that the largest wavelength tuning range achieves 44.2 nm, and the maximum orthogonal polarization suppression ratio (OPSR) is 33.4 dB (TE-type) and 38.7 dB (TM-type).

Keywords: sub-wavelength grating, polarization mode, tunable VCSEL, wavelength tuning

PACS: 42.55.Px

DOI: 10.1088/1674-1056/ab9442

1. Introduction

Tunable vertical-cavity surface-emitting lasers (VCSELs) have attracted great interest in many applications because of their low power consumption, single longitudinal mode, continuous wavelength tuning characteristics.^[1] Especially, in optical communications, tunable VCSELs with polarization stabilization characteristics and wide wavelength tuning range could effectively improve the stability and rate of transmission information.^[2,3] The output wavelength of a tunable VCSELs can be tuned by reducing the thickness of the air gap. However, the wavelength tuning range is hard to increase due to the high reflectivity between the semiconductor cavity and the air cavity. In addition, because of the cylindrical symmetry and isotropic material properties of the device, the polarization behavior of tunable VCSELs could not be fixed reliably.^[4,5] When the temperature and injection current is changed, the polarization mode will randomly be switched between TE and TM. Therefore, tunable VCSELs with polarization stabilization and wide wavelength tuning ranges are a research hotspot. Bakker *et al.*^[6] developed a VCSEL structure with asymmetric current injection; the polarization direction was controlled in the larger current injection. Frasukiewicz *et al.*^[7] and Belmonte *et al.*^[8] developed a 1550 nm liquid-crystal tunable VCSEL, the output wavelength and polarization can be adjusted by tuning the voltage to control the deflection angle of the liquid crystal. This structure has the advantages of small tuning voltage and stable polarization. Kogel *et al.*^[9] developed a

1550 nm tunable VCSEL with an asymmetric top DBR structure; the top DBR film has different bending angles in two orthogonal directions. Therefore, the anisotropies of TE and TM could be increased, with the wavelength tuning range 76 nm. Gründl *et al.*^[10] developed a 1550 nm tunable VCSEL with a sub-wavelength grating (SWG). The SWG was written on the top-DBR mirror and facing the output surface of the VCSEL after two-chip mounting process, the polarization stable wavelength tuning was 25 nm. Chang-Hasnain *et al.*^[11] developed a 1060 nm tunable VCSEL using a high-contrast grating (HCG) as the top mirror. The loss between the two polarization was increased using a high-contrast grating; the wavelength tuning range reached 76 nm. The 850 nm and 1550 nm tunable HCG-VCSELs have also been demonstrated in previous reports.^[12–14]

Sub-wavelength structures have found numerous applications in different optical fields due to their special shapes and optical properties, such as polarization elements,^[15] and diffraction gratings.^[16] In addition, the new nanolithography technique for fabricating various subwavelength structures is also improved constantly.^[17]

In this study, we design a tunable VCSEL structure at 850 nm with an internal-cavity sub-wavelength grating (ISWG) to achieve a wider wavelength tuning range and more stable single-polarization.

*Project supported by the Jilin Science and Technology Development Plan, China (Grant Nos. 20180519018JH and 20190302052GX), Jilin Education Department "135" Science and Technology, China (Grant No. JJKH20190543KJ), the National Natural Science Foundation of China (Grant No. 11474038), and the Key Project of Equipment Pre-Research Fund of China (Grant No. 61404140103).

[†]Corresponding author. E-mail: zouyg@cust.edu.cn

[‡]Corresponding author. E-mail: gjliu626@126.com

[§]Corresponding author. E-mail: mxh@cust.edu.cn

2. Design of the tunable VCSEL with ISWG

The rigorous coupled-wave theory is used to study the polarization characteristics of the sub-wavelength grating.^[18,19] The sub-wavelength grating model is shown in Fig. 1. The incident direction of the light is perpendicular to the sub-wavelength grating. The electric field direction of TE polarization is defined along the grating ridge. The TM polarization mode is defined perpendicular to the grating ridge.

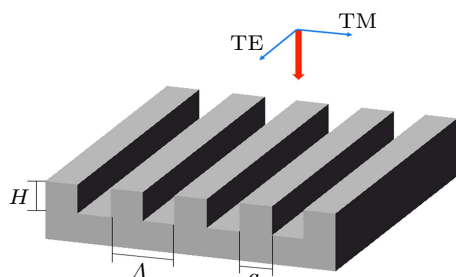


Fig. 1. Sub-wavelength grating structure. GaAs is the grating material, Λ is the period, H is the depth, a is the ridge width, and $f = a/\Lambda$ is the duty cycle.

The high-order diffracted light will exist in the grating when the ratio of the grating period to the wavelength exceeds the critical point. Figure 2 shows the simulation results of critical points when $f = 0.5$ and $H = 100$ nm. Therefore, for

specific incident wavelength, the maximum period of the sub-wavelength grating can be determined.

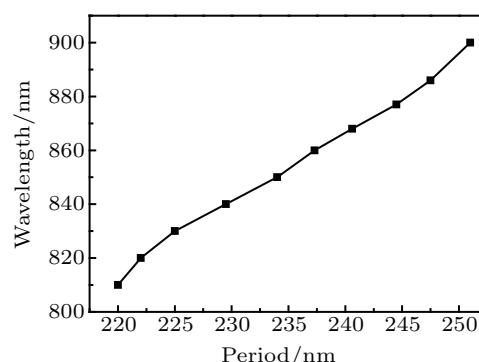


Fig. 2. The relationship between the period of sub-wavelength grating and wavelength when only zero-order diffraction light exists.

The transmittance of sub-wavelength grating with different parameters is calculated as shown in Fig. 3. It can be seen that the sub-wavelength grating has obvious anisotropy between the TE and TM polarization modes. By optimizing the sub-wavelength grating parameters (duty cycle and ridge height), the transmittance of TE (or TM) polarization mode can be greater than 99.99%. At the same time, the transmittance of TM (or TE) polarization is only around 70%.

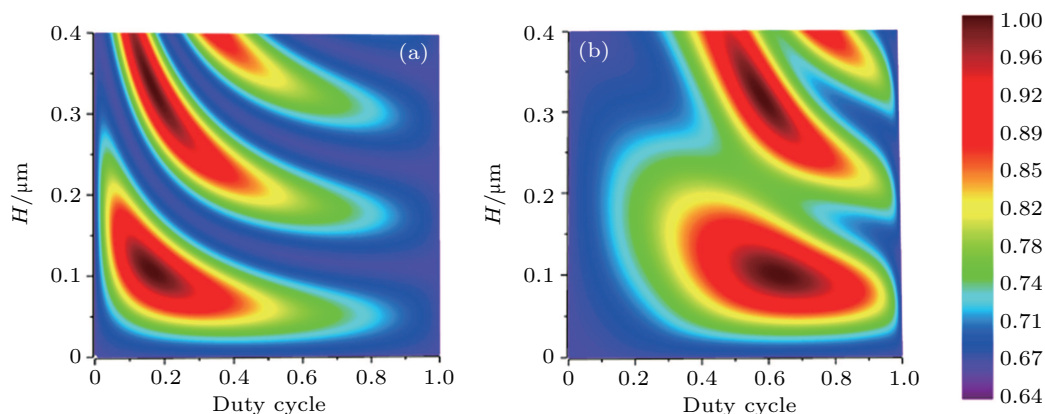


Fig. 3. The effect of ridge height and duty cycle to the transmittance of TE (a) and TM (b) polarization. When the duty ratio is 0.1–0.32 or 0.5–0.84, H is 80–135 nm. The two polarization modes can always maintain a significant difference in the effective index and transmittance.

The influence of grating shape on polarization characteristics should also be considered. A trapezoidal sub-wavelength grating model is built to analyze the effect of sidewall angles on the transmittance of two polarization, as shown in Fig. 4.

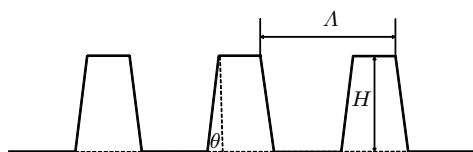


Fig. 4. The schematic diagram of a trapezoidal sub-wavelength grating. Λ is the period, H is the ridge height, and θ is the inclination angle.

The transmittance of sub-wavelength grating with different polarization types is calculated, as shown in Fig. 5. The transmittance of the sub-wavelength grating decreases with

decreasing θ . For $\theta > 75^\circ$, the transmittance of TM-type sub-wavelength grating is more than 95%, and the transmittance difference between the two polarization modes is more than 27%. For $\theta > 78^\circ$, the transmittance of TE-type sub-wavelength grating is greater than 95% and the transmittance difference between the two polarization modes is always larger than 20%. Based on the above analysis, in the range of $\Delta\theta < 10^\circ$, the sub-wavelength grating still has excellent polarization characteristics. The error range is acceptable for using ICP to etch the GaAs material.

The tunable VCSEL structure with an internal-cavity sub-wavelength grating is shown in Fig. 6. It consists of two parts; one part includes 34 pairs of $\text{Al}_{0.9}\text{Ga}_{0.1}\text{As}/\text{Al}_{0.15}\text{Ga}_{0.85}\text{As}$ bottom N-DBRs, a λ -cavity ac-

tive region with 4 $\text{In}_{0.1}\text{GaAs}/\text{Al}_{0.2}\text{GaAs}$ quantum wells, a 50 nm $\text{Al}_{0.98}\text{Ga}_{0.02}\text{As}$ oxidation layer, two pairs of $\text{Al}_{0.9}\text{Ga}_{0.1}\text{As}/\text{Al}_{0.15}\text{Ga}_{0.85}\text{As}$ middle P-DBRs, GaAs cladding layer and sub-wavelength grating structure (etched on the GaAs cladding layer) as a half-VCSEL structure. The period, duty cycle and depth of the TE-type sub-wavelength grating are 220 nm, 0.18 and 105 nm, respectively, and those of the TM-type are 220 nm, 0.65 and 100 nm. The tunable VCSEL with TE(TM)-type sub-wavelength grating, the polarization behavior of device changes to TE(TM) mode. The other part is composed of 20 pairs of $\text{Al}_{0.9}\text{Ga}_{0.1}\text{As}/\text{Al}_{0.15}\text{Ga}_{0.85}\text{As}$ top N-DBRs and a 200 nm $\text{In}_{0.5}\text{Ga}_{0.5}\text{P}$ sacrificial layer as an MEMS cantilever structure. The half-VCSEL structure and the DBR cantilever structure are fabricated. The two parts are bonded together to form a tunable VCSEL structure with an internal-cavity sub-wavelength grating. When the voltage is applied to the tuning electrode of the MEMS cantilever, the air gap is reduced and hence laser wavelength blue shifts.

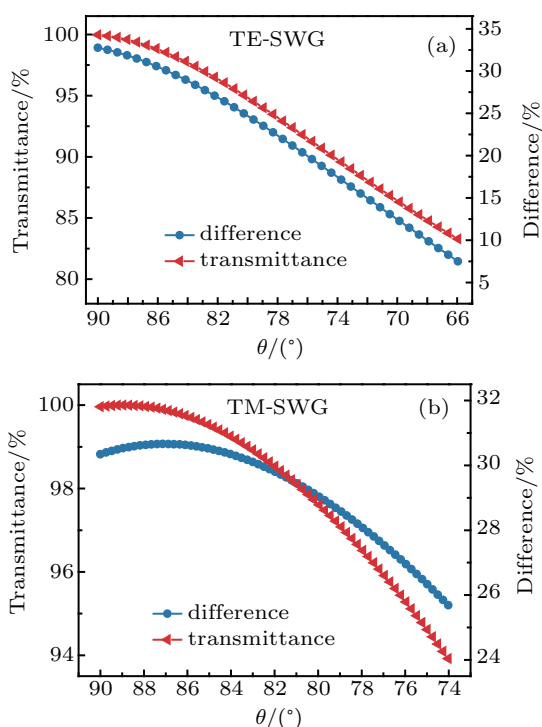


Fig. 5. The effect of θ on the transmittance and difference of polarization mode with the TE-type sub-wavelength grating (a) or the TM-type sub-wavelength grating (b).

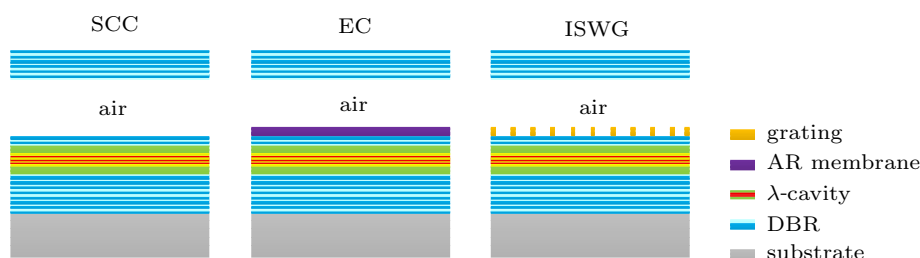


Fig. 7. The schematics of the tunable VCSELs with the SCC, EC, and ISWG structures, respectively.

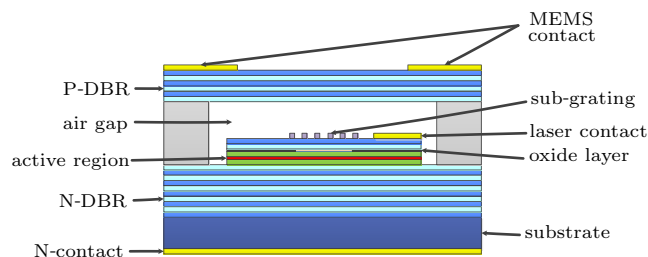


Fig. 6. Schematic cross section of the tunable VCSEL with an internal-cavity sub-wavelength grating.

3. Characterization

3.1. Wavelength tuning

We compared the wavelength tuning characteristics of the internal-cavity sub-wavelength grating (ISWG) structure with semiconductor coupled-cavity (SCC) structure and extended cavity (EC) structure. The schematic diagram of three tunable VCSEL structures are shown in Fig. 7. The ISWG-VCSEL structure is set to output TE polarization mode. All the three cases use the same full layer structures although the structures are different only in their topmost layers beneath the air. The thickness of air gap is set to 1.7 μm .

The wavelength tuning range of the three coupling types of the tunable VCSEL is calculated, as shown in Fig. 8. The resonance wavelengths of the three structures are different at the initial air gap. Therefore, the thickness of air gap at 850 nm is uniformly defined as the center position. The results show that the wavelength tuning ranges are 44.2 nm (ISWG), 36.2 nm (EC), 23 nm (SCC), respectively. Compared with the other structures, the wavelength tuning efficiencies of the ISWG structure are increased by 36.4% (EC) and 92.2% (SCC), respectively. The light field of SCC is confined in the semiconductor cavity because of the high reflection between the interface of semiconductor and air. It causes that the free spectral range (FSR) of tunable VCSEL is significantly limited. With the EC structure, the original semiconductor cavity “extends” into the air gap, the tuning range is 36.2 nm. However, the EC structure does not achieve the best coupling performance during the wavelength tuning process. Compared with the EC structure, ISWG has better coupling performance and wider wavelength tuning range. Additionally, the tuning behavior of the tunable VCSEL with the ISWG structure is linear; and the tuning efficiency is also increased.

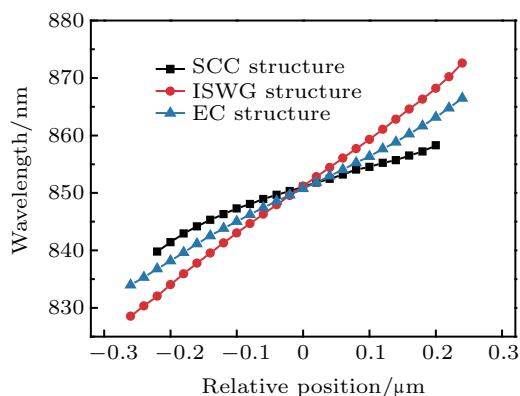


Fig. 8. The relationship between air gap change and output wavelength.

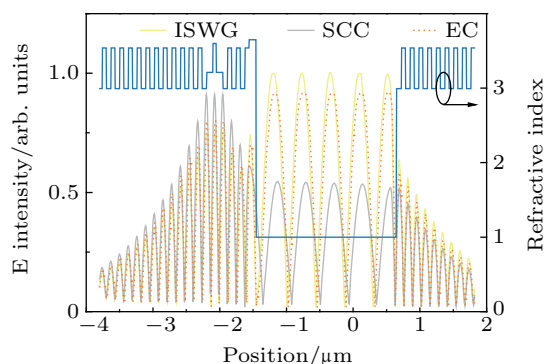


Fig. 9. Electric field intensity distribution.

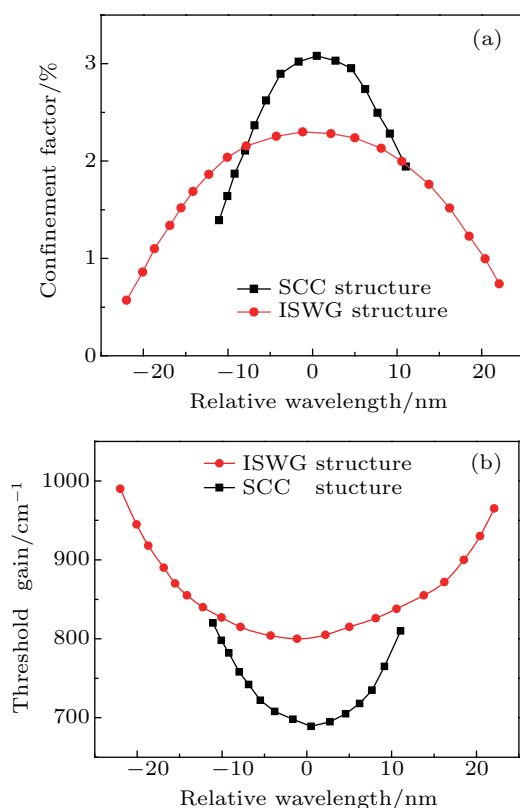


Fig. 10. The confinement factor (a) and the threshold gain (b) of the tunable VCSEL with SCC and ISWG structures, respectively.

Figure 9 shows the distribution of electric field intensity of the tunable VCSEL with SCC, EC, and ISWG, respectively.

The EC and ISWG effectively reduce the reflectivity between the semiconductor and the air. More light energy into the air cavity, the coupling efficiency between the semiconductor and the air is increased. Therefore, the EC and ISWG have a similar distribution of electric field intensity. To further illustrate the effect of the ISWG structure, the longitudinal energy confinement factor Γ and threshold gain are studied. The calculation results are shown in Fig. 10. In this case, the energy confinement factor of the tunable VCSEL is peaked at $\sim 2.4\%$ (ISWG) and 3% (SCC). Despite the significantly lower confinement factor of the tunable VCSEL structure with ISWG, the threshold gain is only increased $\sim 16.3\%$. Because the internal loss is reduced by confining more light energy in the lossless air gap. As a result, using the tunable VCSEL with an internal-cavity sub-wavelength grating, the tuning range is effectively extended while the threshold gain is not compromised significantly.

To illustrate the effect of sub-wavelength grating on wavelength tuning efficiency. According to Eq. (1), the resonant condition of the tunable VCSEL wavelength is analyzed,

$$\frac{4\pi}{\lambda} \left(L_{\text{bot}} + \sum_{i=1}^N n_i d_i + L_{\text{top}} + L_{\text{air}} + L_{\text{mid}} \right) + \theta_{\text{top}} + \theta_{\text{bot}} = 2\pi m, \quad (1)$$

where θ_{top} and θ_{bot} are the reflection phases of the top and bottom DBR; n_i and d_i are the refractive index and thickness of each layer; L_{top} , L_{bot} , and L_{mid} are the effective lengths of the top, bottom, and intermediate DBR, respectively. Especially, θ_{top} , L_{air} , and θ_{bot} are the primary influence on the wavelength tuning. The variables of L_{air} and θ_{bot} in the three structures during wavelength tuning are the same. However, θ_{top} 's of the three structures are different due to the different coupling mechanisms of the light field; the calculation results are shown in Fig. 11. From the results, θ_{top} in the ISWG structure has the most considerable change. When the variables of air gap are the same, the tunable VCSEL with the ISWG structure has more significant wavelength changes and its wavelength tuning efficiency rises.

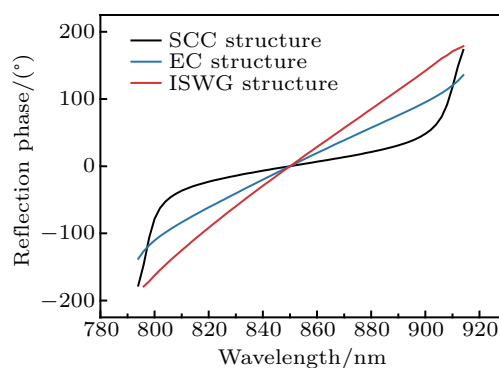


Fig. 11. The relationship between θ_{top} and wavelength of the three structures.

3.2. Polarization characteristics

To illustrate the polarization characteristics of the tunable VCSEL with the ISWG structure, we study the resonant wavelengths of two polarization modes for different air gaps. The influence of grating etching error ($\theta = 90^\circ, 85^\circ, \text{ and } 80^\circ$) on wavelength separation is also analyzed; the results are shown in Fig. 12. To illustrate the effect of wavelength separation between TE and TM on the polarization characteristics, the threshold gains for TE-type tunable VCSEL and TM-type tunable VCSEL are calculated, as shown in Fig. 13.

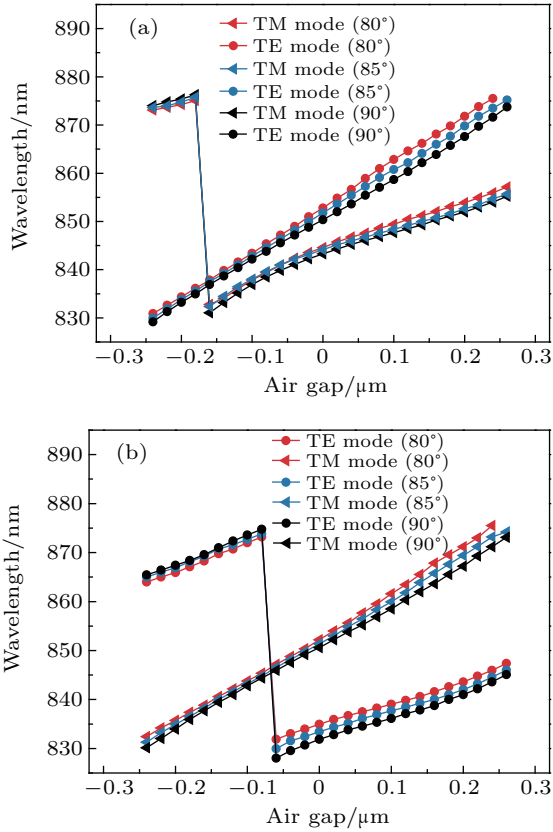


Fig. 12. The wavelength tuning range of the two polarization modes for the TE-type (a) and TM-type (b) tunable VCSEL, respectively, when θ is different.

For TE-type tunable VCSEL structures, the maximum wavelength separation of the two polarization modes is 17.5 nm; the wavelength separation is always higher than 4 nm. For the TM-type tunable VCSEL structures, the maximum wavelength separation of the two polarization modes is 28 nm, the wavelength separation is still higher than 17.6 nm. At the same time, we observe that there are little dependences of the polarization characteristics and wavelength tuning range of tunable VCSEL on the grating shape. With θ in 80° – 90° , the TE and TM polarization always maintain a significant value of wavelength separation. For the TE-type tunable VCSEL structures, the TM polarization can be suppressed effectively because of the threshold gain of TE is always smaller

than TM. The switching phenomenon between TE and TM polarizations is avoided. Compared with the TE-type tunable VCSEL structure, the TM-type tunable VCSEL structure has a more significant threshold gain difference, especially near the central wavelength. Therefore, the TM-type tunable VCSEL structure has a stronger suppression ability for the TE polarization. In the case of low current injection, the results show that the tunable VCSEL structures with different types of sub-wavelength gratings can effectively avoid the polarization switching during wavelength tuning.

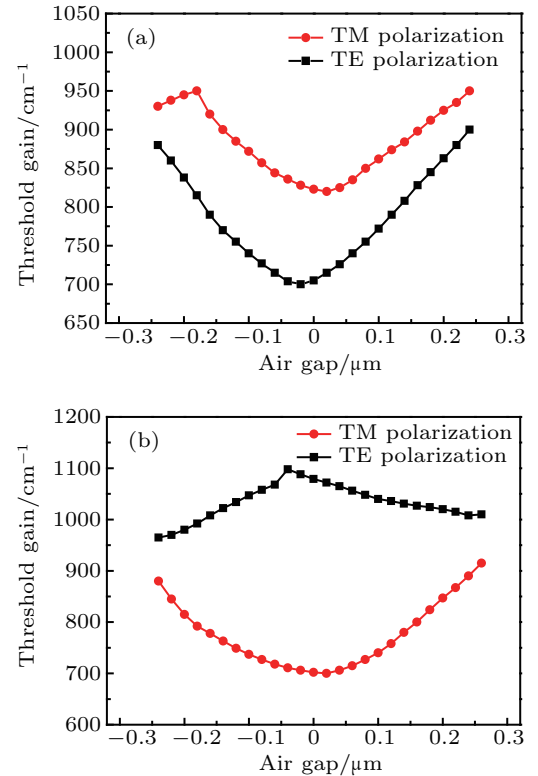


Fig. 13. The relationship between threshold gain and different polarization modes for the TE-type tunable VCSEL (a) and the TM-type tunable VCSEL (b).

For the central wavelength of 850 nm, the orthogonal polarization suppression ratio (OPSR) with different injection currents is calculated by

$$\text{OPSR} = 10 \log \left(\frac{P_1}{P_2} \right), \quad (2)$$

where P_1 and P_2 are the output powers of the two polarization modes, respectively. The results are shown in Fig. 14. The maximum OPSRs are 33.4 dB (TE-type) and 38.7 dB (TM-type). As the current injection increases, the OPSR decreases because of the self-heating. However, the OPSR is always greater than 28 dB (TE-type) and 31.2 dB (TM-type), which indicates that the switching between the two polarization modes is effectively suppressed.

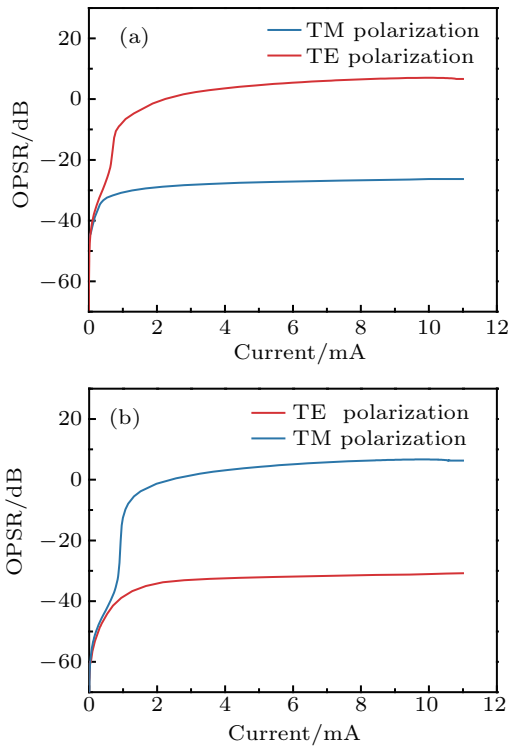


Fig. 14. At different injection currents, the OPSRs of the TE-type tunable VCSEL (a) and the TM-type tunable VCSEL (b).

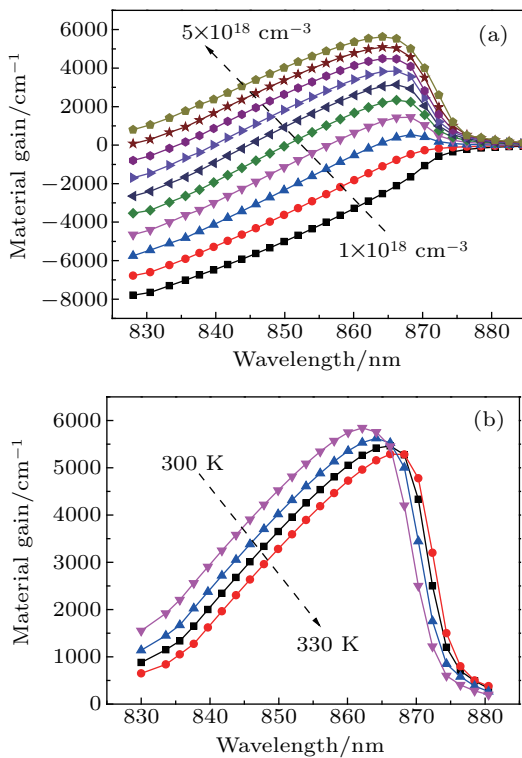


Fig. 15. The material gain curve with different carrier concentrations (a) and temperatures (b).

The resonance wavelength, which is close to the material gain peak, can obtain high quantum well gain and play a dominant role in the mode competition. The degree of suppression between modes is proportional to the difference in relative gain. Combined with the material gain spectrum and

wavelength separation state, the polarization mode characteristic with high current injection during the wavelength tuning is analyzed. Figure 15 shows the material gain spectrum of the active region corresponding to different carrier concentrations and different temperatures.

For the TE-type tunable VCSEL structures, the resonant wavelength of the TM polarization mode is switched from 832.3 nm to 875.8 nm. However, the TM polarization mode still has a lower quantum well gain compared to the TE polarization mode. Therefore, the tunable VCSEL can maintain stable TE polarization during the wavelength tuning. Because the TM-type tunable VCSEL structure has a more significant value of wavelength separation, it has a higher polarization suppression ability. However, when the tuning wavelength of the TM polarization mode is 840 nm, the gains for the TM and TE polarization modes are close to each other, the competition between polarization modes increases, the polarization suppression ability of the device decreases. When the TM tuning wavelength is less than 840 nm, the TE polarization mode plays a dominant role in mode competition and the mode hopping will incur in the device. The results show that the TE-type tunable VCSEL structure has stable single-polarization output characteristics in the process of continuous wavelength tuning. The TM-type tunable VCSEL structure has the most stable output characteristics of a single polarization mode near the low current injection. However, at the high current injection, the wavelength tuning range of stable polarization mode is smaller than the TE-type tunable VCSEL structure.

4. Conclusions

We have designed an 850 nm tunable VCSEL structure with internal-cavity sub-wavelength grating (ISWG). The effects of sub-wavelength grating's parameters (period, duty cycle, ridge height) on the transmittance and effective index of the two polarization modes (TE/TM) are analyzed. The results show that the subwavelength grating has good polarization characteristics and large tolerance, so the difficulty of fabrication can be reduced to some extent. We theoretically study the optical characteristics of tunable VCSEL structures with three different coupling types and it is demonstrated that the ISWG structure is significantly effective for increasing the wavelength tuning range. In addition, we calculate the polarization power and threshold gain characteristics of such an ISWG VCSEL and show the possibility of achieving a single-polarization mode within the wavelength tuning range. In the fabrication process, the thickness variation of the bonding material before and after curing needs to be considered, which will affect the output wavelength and free spectral range of the device. The results show the largest wavelength tuning range achieves 44.2 nm. The maximum orthogonal polarization suppression ratio (OPSR) is 33.4 dB (TE-type) and 38.7 dB (TM-

type), respectively. It is shown that the tunable VCSEL with ISWG could achieve stable polarization, and eliminate the defect of polarization mode instability.

References

- [1] Iga K 2008 *Jpn. J. Appl. Phys.* **47** 1
- [2] Xiang L, Zhang X, Zhang J W, Huang Y W, Ning Y Q and Wang L J 2018 *Chin. Phys. B* **27** 074210
- [3] Liu A, Wolf P, Lott J A and Bimberg D 2019 *Photon. Res.* **7** 121
- [4] Chen J J, Xia G Q and Wu Z M 2015 *Chin. Phys. B* **24** 024210
- [5] Xun M, Xu C, Xie Y Y, Deng J, Xu K, Jiang G Q, Pan G Z and Chen H D 2015 *Chin. Phys. Lett.* **32** 104204
- [6] Bakker M P, Barve A V, Zhan A, Coldren L A, Van Exter M P and Bouwmeester D 2014 *Appl. Phys. Lett.* **104** 151109
- [7] Frasunkiewicz L, Czyszanowski T, Thienpont H and Panajotov K 2018 *Opt. Commun.* **427** 271
- [8] Belmonte C, Frasunkiewicz L, Czyszanowski T, Thienpont H, Beeckman J, Neyts K and Panajotov K 2015 *Opt. Express* **23** 15706
- [9] Jatta S, Kögel B, Maute M, Zogal K, Riemenschneider F, Böhm G and Amann M C 2009 *IEEE Photon. Technol. Lett.* **21** 1822
- [10] Grundl T, Zogal K, Debernardi P, Muller M and Meissner P 2013 *IEEE Photon. Technol. Lett.* **25** 841
- [11] Qiao P, Cook K, Li K and Chang-Hasnain C J 1995 *IEEE J. Sel. Top. Quantum Electron.* **1** 1
- [12] Rao Y, Yang W, Chase C and Huang M C Y 2013 *IEEE J. Sel. Top. Quantum Electron.* **19** 1701311
- [13] Huang M C Y, Zhou Y and Chang-Hasnain C J 2008 *Nat. Photon.* **2** 180
- [14] Yang W, Zhu L, Rao Y, Chase C, Huang M and Chang-Hasnain C J 2013 *IEEE Avionics, Fiber-Optics and Photonics Technology Conference (AVFOP)*, San Diego, CA, USA, October 1–3, 2013, pp. 86-87
- [15] Chou S Y and Deng W 1995 *Appl. Phys. Lett.* **67** 742
- [16] Moore C P and Beard W L 2017 *INT J. Nanotechnol* **14** 297
- [17] Pang Z Y, Tong H, Wu X X, Zhu J K, Wang X X, Yang H and Qi Y P 2018 *Opt. Quantum Electron.* **50** 335
- [18] Kanamori Y, Roy E and Chen Y 2005 *Microelectron. Eng.* **78–79** 287
- [19] Carr D W, Sullivan J P and Friedmann T A 2003 *Opt. Lett.* **28** 1636